

Modeling hemodynamics in an unoccluded and partially occluded inferior vena cava under rest and exercise conditions

Zhuyin Ren · Stephen L. Wang · Michael A. Singer

Received: 2 July 2011 / Accepted: 6 February 2012 / Published online: 22 February 2012
© International Federation for Medical and Biological Engineering (outside USA) 2012

Abstract Pulmonary embolism is the third leading cause of death in hospitalized patients in the US. Vena cava filters are medical devices inserted into the inferior vena cava (IVC) and are designed to trap thrombi before they reach the lungs. Once trapped in a filter, however, thrombi disturb otherwise natural flow patterns, which may be clinically significant. The goal of this work is to use computational modeling to study the hemodynamics of an unoccluded and partially occluded IVC under rest and exercise conditions. A realistic, three-dimensional model of the IVC, iliac, and renal veins represents the vessel geometry and spherical clots represent thrombi trapped by several conical filter designs. Inflow rates correspond to rest and exercise conditions, and a transitional turbulence model captures transitional flow features, if they are present. The flow equations are discretized and solved using a second-order finite-volume method. No significant regions of transitional flow are observed. Nonetheless, the volume of stagnant and recirculating flow increases with partial occlusion and exercise. For the partially occluded vessel, large wall shear stresses are observed on the IVC and on the model thrombus, especially under exercise conditions.

These large wall shear stresses may have mixed clinical implications: thrombotic-like behavior may initiate on the vessel wall, which is undesirable; and thrombolysis may be accelerated, which is desirable.

Keywords CFD · Filter · Thrombosis · Vena cava · Wall shear stress

1 Introduction

Pulmonary embolism (PE) is a serious medical condition that presents in approximately 900,000 patients annually; nearly one-third of cases are fatal [19, 31]. Most frequently, PE is the result of venous thrombi that dislodge from the deep veins in the lower extremities and travel to the lungs. En route to the lungs, blood from the lower extremities flows through the bilateral iliac veins before traversing the inferior vena cava (IVC). Flow through the IVC then merges with inflow from the renal veins before reaching the right atrium of the heart.

All blood from the deep venous system of the lower extremities, which may contain deadly deep vein thrombosis (DVT), flows through the IVC. Consequently, medical devices that prevent DVT from reaching the heart are most frequently inserted into the IVC. In doing so, these devices, called IVC filters, are designed to intercept and trap large clots while allowing clot-free blood to bypass freely. Inferior vena cava filters are a routine clinical treatment for the prevention of PE, particularly in patients who have contraindications to anticoagulation. Approximately 100,000 filters are deployed annually in the US [16].

Upon trapping thrombus in the filter, the IVC becomes partially occluded, and the flow disruption impacts the local hemodynamics significantly. As demonstrated both

Z. Ren
Department of Mechanical Engineering,
University of Connecticut, Storrs, CT 06269, USA

S. L. Wang
Division of Vascular and Interventional Radiology,
Kaiser Permanente Santa Clara Medical Center,
Santa Clara, CA 95051, USA

M. A. Singer (✉)
Center for Applied Scientific Computing,
Lawrence Livermore National Laboratory,
P.O. Box 808, L-422, Livermore, CA 94551, USA
e-mail: msinger2006@gmail.com

in-vitro (e.g., [8, 10, 14, 15, 28]) and with computational models (e.g., [22, 24, 25, 27, 29, 34]), partial occlusion of the IVC impacts both the flow dynamics (e.g., volume of stagnant/recirculating flow) and the wall shear stress (WSS), and unnatural flow patterns may elevate the risk of thrombosis [12, 17]. Therefore, a thorough characterization and understanding of the hemodynamics of the partially occluded IVC is essential for assessing the potential risks and benefits of vena cava filters.

One aspect of IVC hemodynamics that is particularly disconcerting is the potential for transitional and turbulent flow. The presence of transitional or turbulent blood flow may result in endothelial cell damage [11], and turbulence can contribute to the formation of thrombi [26]. Further, turbulence may cause vessel damage and facilitate hemolysis [18]. Consequently, partially occluded IVC filters that induce transitional or turbulent flow are best avoided. In the context of currently deployed filters that trap thrombus in the center of the IVC (e.g., G2 (Bard Peripheral Vascular, Tempe, AZ), Celect (Cook, Bloomington, IN), Gunther Tulip (Cook)), regions of high-speed flow are observed in the narrow passage between the thrombus and the vessel wall. Can these regions of jet-like flow lead to clinically significant transitional or turbulent flow downstream of the clot? Addressing this question and the overall hemodynamic environment inside the IVC under rest and exercise conditions are the foci of this work.

This study examines the flow in an unoccluded and partially occluded IVC under rest and exercise conditions. Flow characteristics are obtained using computational fluid dynamics (CFD) combined with a realistic model of the IVC and surrounding vasculature (i.e., iliac and renal veins). An idealized computer model is constructed from patient-specific computed tomography (CT) scan data, and iliac and renal inflow conditions are obtained from in-vivo data from the literature. All vessel walls are taken to be rigid, and thrombi are modeled as rigid spheres, which, in some sense, represent an average shape of thrombus observed in the clinical setting [29]. During a normal cardiac cycle, the cross section of the IVC changes by approximately 1.4 and 1 mm in the short and long axis, respectively [20]. Though the computer model represents a simplified abstraction of the complex physiology that surrounds the real IVC, it contains the essential physical elements that determine the overall flow pattern (e.g., iliac and renal inflow, elliptical cross-section), especially those that may promote or inhibit the onset of transitional flow.

2 Methods

A realistic, three-dimensional model of the IVC, iliac, and renal veins is used to represent the physiology (Fig. 1) (see

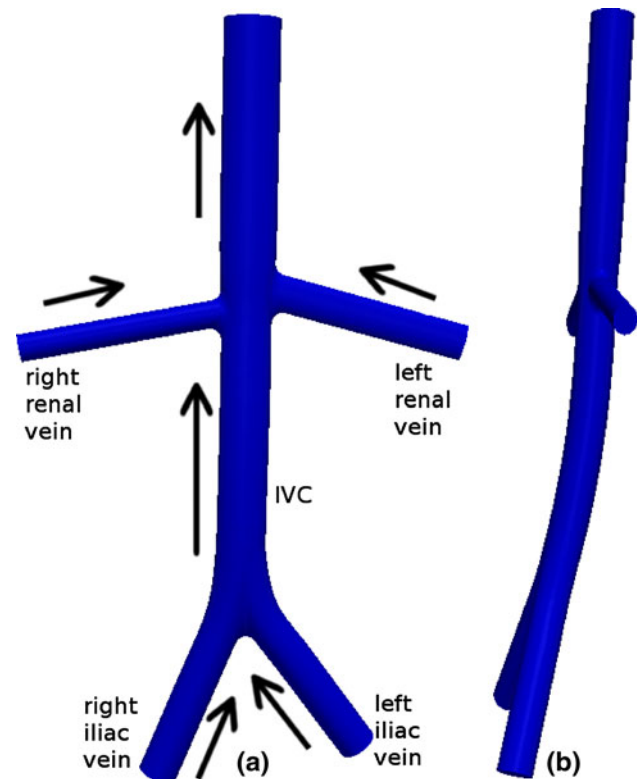


Fig. 1 Schematic of the computer model used to represent the IVC and surrounding vessels: **a** front view and **b** side view. The *arrows* indicate the direction of flow. Note the use of the radiological *right* and *left* to denote the iliac and renal veins

Ref. [24] for a schematic diagram that contains a model thrombus and IVC filter). For this study, the geometrical model is identical to that used in [22], which was constructed from 10 CT scan data sets of patients with conventional vena cava anatomy. Entry angles of the bilateral renal and common iliac veins into the IVC were calculated and averaged using the CT scan data sets. Average cross-sectional dimensions of the veins and the IVC were also calculated and used to construct the ellipsoidal cross-sectional shapes of all vessels.

The computational model is meshed using uniform tetrahedral meshes with attached, non-uniform hexahedral meshes at all solid walls. The hexahedral grids capture the viscous flow dynamics near the vessel walls, and the local grid spacing is adjusted to ensure that at least five grid points are in the boundary layer (recommended grid resolution in Ref. [2]). In total, the mesh contains approximately 3 million grid cells. A grid refinement study showed the use of hybrid meshes (i.e., tetrahedral and hexahedral) ensures that the boundary layers and wakes are well-resolved while minimizing the computational expense. In particular, adequate grid refinement is used to ensure resolution of the WSS.

Fluid flow analysis is performed using ANSYS Fluent, which is a commercial CFD solver suitable for a wide

variety of compressible and incompressible flow problems [1]. Blood is modeled as a homogeneous, incompressible, Newtonian fluid with density $\rho = 1,040 \text{ kg/m}^3$ and dynamic viscosity $\mu = 2.57 \times 10^{-3} \text{ kg/ms}$. From the work of Swaminathan et al. [29], the Newtonian approximation is appropriate for the current flow regime: non-Newtonian effects are minimal, and the Newtonian approximation is often used for modeling flow through the IVC [24, 25, 27, 34]. The flow obeys the conservation of mass and momentum as described by the incompressible Navier–Stokes equations, which are discretized using a second-order finite-volume method (in space) as described in [2].

To model flow in the boundary layers and to capture the possible transition from laminar to turbulent flow, the $k\text{--}kl\text{--}\omega$ transition model is used [32]. This computational model is based on the eddy-viscosity hypothesis and is well-suited for transitional flows. To compute the eddy-viscosity and therefore fully describe the flow, the model solves three additional transport equations: one for the turbulent kinetic energy (k), which describes the energy in the turbulent flow field; one for the laminar kinetic energy (kl), which describes the energy in the laminar flow field; and one for the inverse turbulent time scale (ω), which provides a time scale that characterizes the turbulent flow field and is used to compute the eddy-viscosity. The flow is taken to be statistically stationary (e.g., unsteadiness due to the cardiac cycle is excluded from the model).

In all of the computations, the SIMPLE scheme is used for pressure–velocity coupling, and second order upwind schemes are used to solve the momentum, turbulent kinetic energy, laminar kinetic energy, and specific dissipation rate equations; the PRESTO scheme is used to compute the pressure.

To assess flow disturbances caused by trapped clots and the possible transition to turbulent flow, model thrombus is inserted into the computational model of the IVC. In all cases, the clots are spherical, which is a representative shape for clots trapped by conical filters, e.g., Celect (Cook, Bloomington, IN), Gunther Tulip (Cook), Greenfield (Boston Scientific, Watertown, MA). The size of the clots is 1.5 mL, which is representative of relatively large thrombus volumes observed in clinical practice [33]. By selecting a large, yet clinically relevant clot size, maximum disturbance to the flow is ensured, thereby increasing flow disruption and the likelihood of transitional or turbulent flow. That is, using a large thrombus represents, in some sense, a worst case scenario for inducing transitional flow. Note that the filter itself is excluded from the current model. As demonstrated throughout the IVC modeling and in-vitro literature (e.g., [14, 24, 27]), the trapped thrombus is the primary source of disrupted flow in partially occluded filters.

Table 1 Inflow rates (L/min) through the iliac and renal veins for the rest, exercise, and high exercise conditions

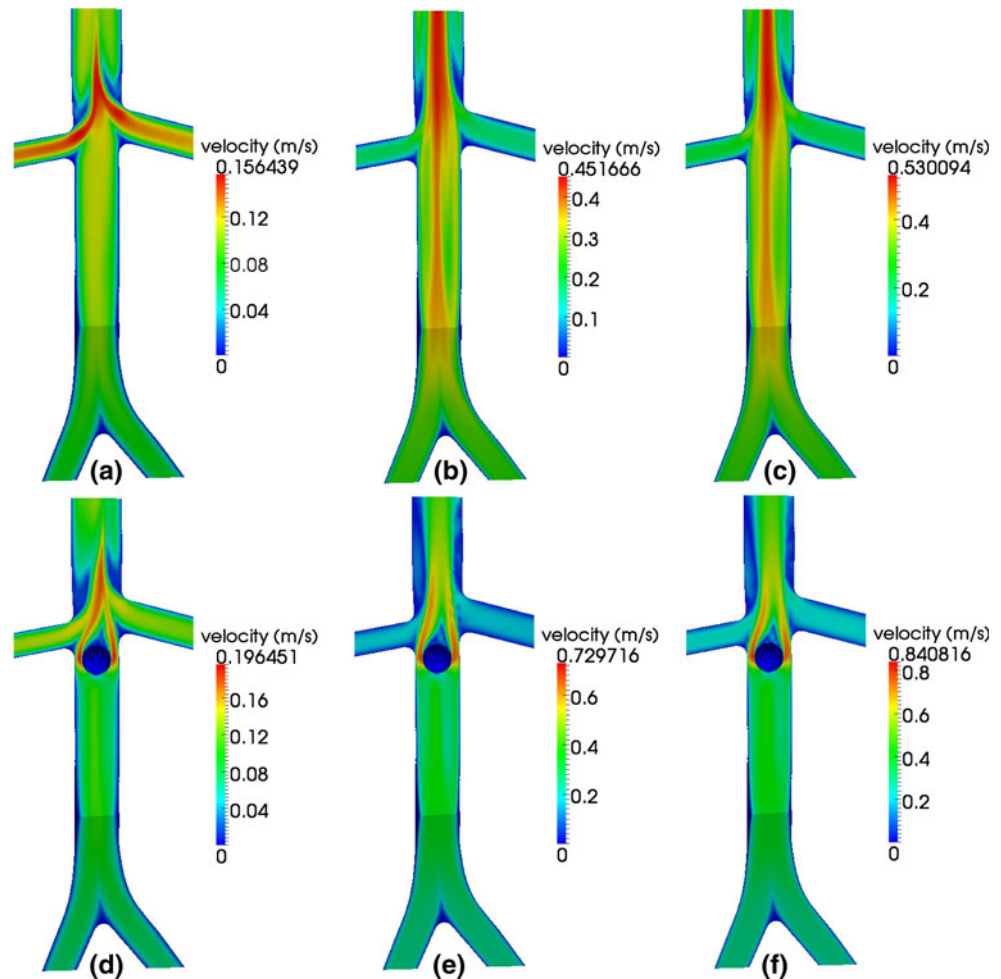
Location	Rest	Exercise	High exercise
Left/right iliac	0.68	2.65	3.1
Left/right renal	0.45	0.60	0.85

The physiologically realistic flow rates listed in Table 1 are specified at the iliac and renal inflow boundaries. The corresponding infrarenal Reynolds numbers for the rest, exercise, and high exercise conditions are approximately 360, 1,400, and 1,640, respectively; the suprarenal Reynolds numbers are approximately 600, 1,720, and 2,090. These flow rates and Reynolds numbers correspond to those observed in-vivo under rest and exercise (on a stationary bicycle) conditions using magnetic resonance imaging [4]. At the inflow boundaries, the laminar kinetic energy, kl , is set to $1 \times 10^{-6} \text{ m}^2/\text{s}^2$, the turbulence intensity is set to 2% of the mean inlet velocity, and the viscosity ratio (the ratio between the turbulent viscosity and the laminar viscosity) is set to 2. A parameter study found that the turbulent inlet properties do not significantly impact flow through the IVC and near the model thrombus. At the outlet boundary of the IVC, a zero gauge pressure is specified.

3 Results

Regions of stagnant flow are observed distal to the renal inflow along the wall of the IVC, and the volume occupied by low-velocity flow increases with flow rate (i.e., exercise). As indicated in Fig. 2, these flow conditions are present in both the unoccluded and the partially occluded vessels. For the cases with no occlusion (i.e., Fig. 2a–c), the peak flow velocity throughout the domain occurs near the center of the IVC, just downstream of the renal inflow. Here, inflow from both renal veins combines with the flow through the IVC. Under exercise conditions (i.e., Fig. 2b–c), however, high-speed flow persists throughout the suprarenal portion of the IVC, which produces a relatively high velocity jet in the center of the vessel and low-speed flow along the vessel walls. The low-speed flow results from the conservation of mass and the no-slip boundary condition on the walls of the vessel. Under rest condition, high-velocity flow in the vicinity of renal inflow is confined to the center of the IVC, and the high-speed jet that contains renal and IVC flow is short-lived as the velocity gradients are smoothed. This smoothing is due to the domination of viscous effects, which induces a loss of flow momentum in the suprarenal portion of the vessel. In all unoccluded cases, regions of low-velocity flow are also observed near the junction of the iliac veins with the IVC.

Fig. 2 Velocity contours for rest (a, d), exercise (b, e), and high exercise (c, f) flow conditions. Unoccluded vessels are in the top row (a–c), and partially occluded vessels are in the bottom row (d–f)



For the unoccluded vessel, the significance of the high-speed renal inflow in determining the suprarenal flow pattern decreases from rest to exercise conditions. Under rest conditions, inflow from the renal veins is large in comparison to infrarenal flow through the IVC. Consequently, renal inflow induces appreciable disruption to the downstream flow through the IVC, which is consistent with the results reported in [34]. For flow under exercise conditions, however, the velocity of flow through the infrarenal IVC is large in comparison to that of the renal veins. As a result, the disruption caused by renal inflow is relatively small, and the tendency is for renal inflow to increase the flow velocity in the center of the vessel (Fig. 2).

Thrombus has a significant impact on flow near the renal veins and in the suprarenal IVC. As indicated in Fig. 2d–f, the peak velocity throughout the flow domain increases (compared to the unoccluded case) by approximately 25 and 60% for the rest and exercise conditions, respectively. In addition, the location of the peak velocity moves from the suprarenal IVC in the unoccluded cases to the narrow passage between the clot and the wall of the IVC for the partially occluded cases.

The volume of low-velocity flow along the wall of the suprarenal IVC increases with vessel occlusion and flow rate (i.e., exercise). For the partially occluded case under rest conditions, the volume of suprarenal vessel occupied by low-velocity flow extends farther downstream than for the corresponding unoccluded vessel (Fig. 2). Nonetheless, low-speed flow is confined to the immediate vicinity downstream of the renal veins. Under exercise conditions, however, high-velocity flow that results from flow bypassing the thrombus is pushed toward the center of the vessel by inflow from the renal veins. As a result, low-velocity flow is observed along the entire wall of the suprarenal IVC.

The wall shear stresses computed by the unoccluded computer model are consistent with those measured in-vivo. In the work of Cheng et al. [4], the mean wall shear stresses for the infrarenal IVC under rest and exercise conditions are $0.20 \pm 0.06 \text{ N/m}^2$ and $0.75 \pm 0.19 \text{ N/m}^2$, respectively. The corresponding wall shear stresses computed from the model are approximately 0.18 and 0.8 N/m^2 , respectively. For suprarenal flow, Cheng et al. [4] report the mean wall shear stresses for rest and exercise

to be $0.34 \pm 0.10 \text{ N/m}^2$ and $1.15 \pm 0.65 \text{ N/m}^2$, respectively. The corresponding shear stresses computed from the model are approximately 0.32 and 1.0 N/m^2 , respectively. The slight discrepancies are likely the result of different vessel geometries and flow pulsatility due to the cardiac cycle, which is present in-vivo but excluded from the computer model. Nonetheless, the quantitative agreement indicates that the computer model captures the velocity gradients along the wall of the vessel, and this agreement further indicates that the model contains sufficient spatial resolution in the viscous boundary layers.

The presence of thrombus increases the WSS significantly, especially under exercise conditions. As indicated in Figure 3, which shows the local WSS on the surface of the vessel (i.e., not circumferentially averaged), the peak WSS of the partially occluded vessel during exercise increases by a factor of approximately 2, 5, and 4.25, for rest, exercise, and high exercise conditions, respectively. In addition, the location of the peak WSS moves as a result of the flow disruption caused by the thrombus. For the unoccluded vessels, the peak WSS is located on the downstream portion of the renal veins, where renal inflow merges with flow through the IVC. In contrast, the peak WSS for the partially occluded vessels is adjacent to the model thrombus, where flow through the IVC bypasses the thrombus by traversing the narrow passage between the clot and the wall of the IVC.

The peak WSS through a normal, unoccluded vessel may increase by a factor of 4 during high exercise, and Fig. 3 suggests that the peak WSS in a healthy, unoccluded IVC may vary from approximately 0.87 N/m^2 for rest to 3.5 N/m^2 for exercise. This quantitative range of wall shear stresses is the first reported in the literature for the IVC and serves as a benchmark by which to assess the clinical significance of venous thrombus on the WSS. That is, for e.g., by comparing the WSS profiles and values for unoccluded vessels under exercise conditions with the corresponding data for partially occluded vessels under rest conditions, a quantitative assessment of the impact of vessel occlusion may be made.

The WSS on the thrombus increases with flow rate, and the peak WSS is located just upstream of the equator. As indicated in Fig. 4, the WSS on the upstream half of the thrombus is larger than the WSS on the downstream half, which is expected due to flow separation on the surface of the clot that leads to low-velocity flow in the wake.

The turbulent kinetic energy (TKE), which measures the mean kinetic energy per unit mass in a turbulent flow field, increases with flow rate (i.e., rest to exercise conditions) and with partial occlusion (Fig. 5). In the present context, TKE is produced by fluid shear and friction at the large, inertial scales of the flow and is transferred down the turbulence energy cascade to the small spatial scales where it

is dissipated by viscosity. Hence, the regions of relatively high TKE correspond to regions of the flow that may be transitional. But, for the unoccluded vessel (Fig. 5a–c) the energy contained in the turbulent flow field is very low in comparison to the total kinetic energy contained in the flow field (e.g., squaring the velocities in Fig. 2), which suggest that the flow is indeed laminar. Note that under rest conditions (i.e., Fig. 5a, d), the maximum TKE is approximately 1.5 times larger for the partially occluded vessel than for the unoccluded vessel, which is due to the model thrombus impacting flow through the right renal vein. Nonetheless, the TKE in the renal veins remains small in comparison to the total kinetic energy in the flow field. For the partially occluded vessel, the TKE increases by more than six orders of magnitude from rest to exercise conditions.

Under exercise conditions (i.e., Fig. 5e–f), the peak values of TKE are located just downstream of the thrombus, which is due to large velocity fluctuations in the wake of the thrombus. There is also elevated TKE in the suprarenal IVC, which is initiated in the thrombus wake and propagates downstream. Elsewhere throughout the flow, the TKE is low.

Streamlines near the renal inflow and thrombus indicate that renal inflow combines smoothly with IVC flow and there is minimal indication of flow reversal near the center of the vessel (Fig. 6). In addition, the wake of the thrombus is localized and does not impact the overall flow pattern significantly. As pictured in Fig. 6, wherein the streamlines are colored by vorticity (which measures the amount of rotation in the flow), the vorticity increases from rest to exercise and also with partial occlusion. For unoccluded flow under rest conditions (Fig. 6a), vorticity is largest in the suprarenal IVC due to rotation introduced by the renal inflow. Unoccluded flow through the infrarenal IVC under exercise conditions (Fig. 6b–c) contains appreciable vorticity due to the relatively high inflow rates from the iliac veins. Peak vorticity in the partially occluded vessel occurs in the narrow passage between the thrombus and the wall of the IVC. Here, vorticity is introduced into the flow due to the viscous effects caused by the no-slip boundary condition on the clot and the vessel wall. Vorticity propagates downstream and is again altered by the renal inflow.

4 Discussion

Flow through the infrarenal IVC under rest conditions is fully developed and reminiscent of Poiseuille flow (Fig. 2a). These regular flow conditions may reduce the risk of IVC thrombosis due to the absence of localized regions of high shear, but may also restrict the ability of oncoming flow to lyse trapped clots. As indicated in Fig. 2,

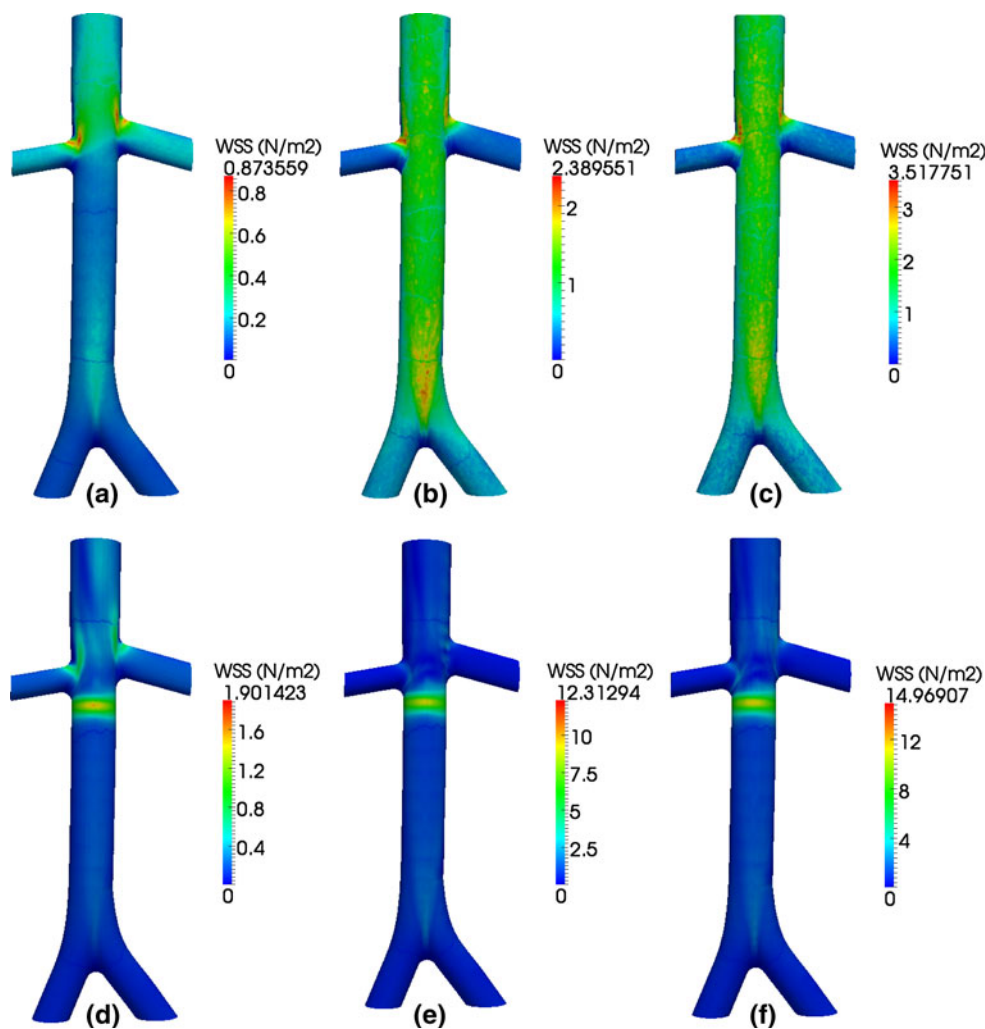


Fig. 3 Wall shear stress (WSS) for rest (a, d), exercise (b, e), and high exercise (c, f) flow conditions. Unoccluded vessels are in the *top row* (a–c), and partially occluded vessels are in the *bottom row* (d–f)

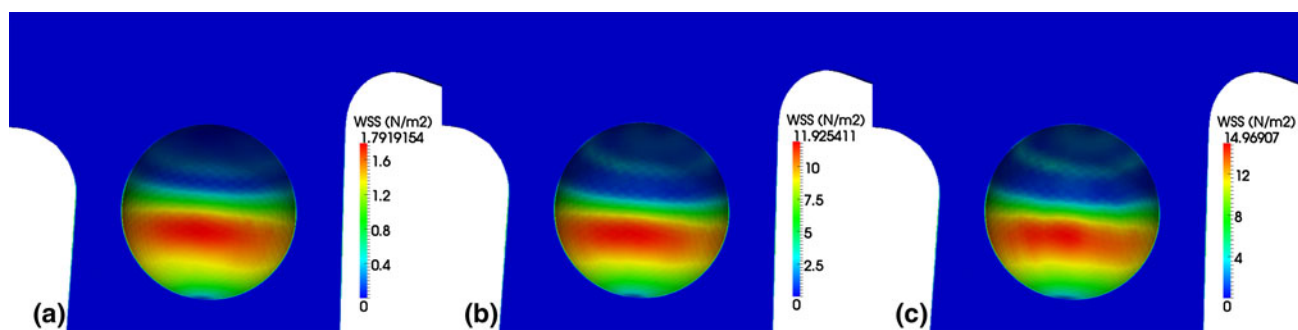
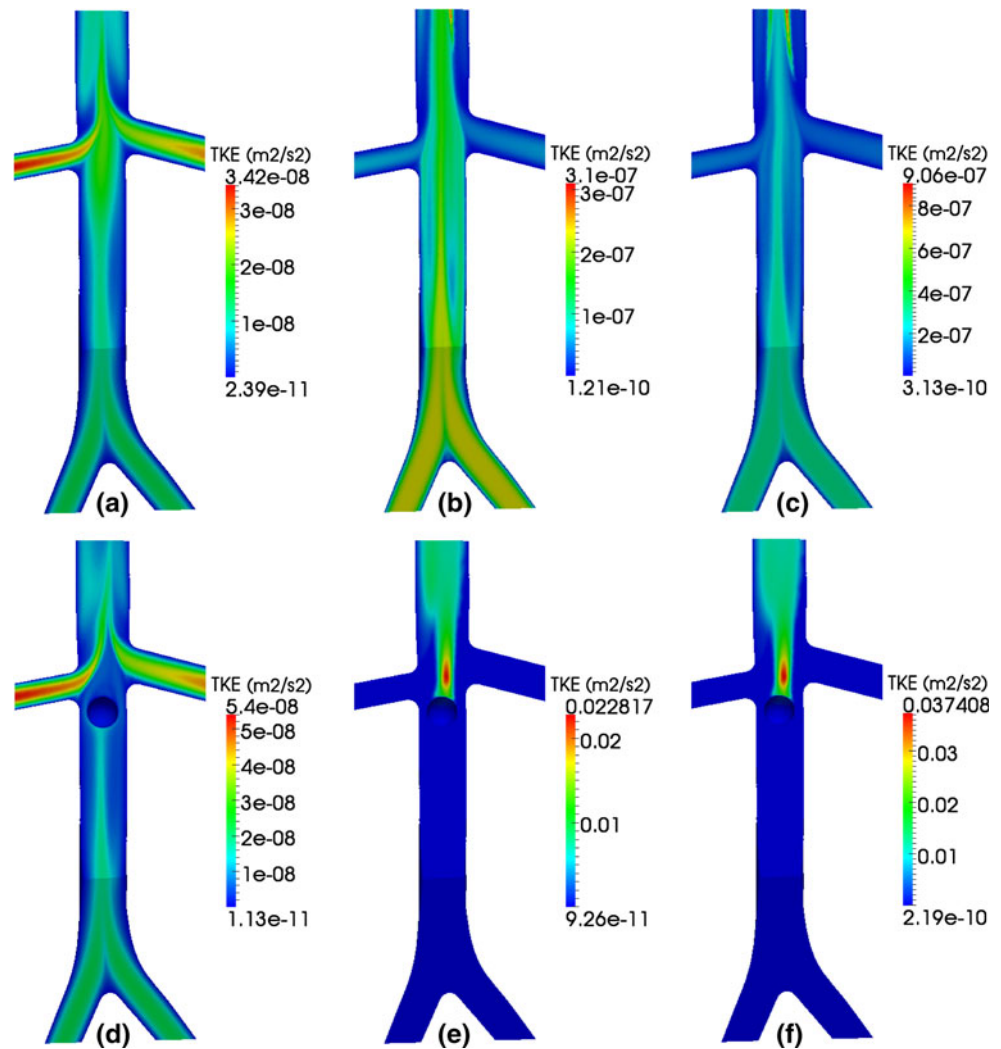


Fig. 4 Wall shear stress (WSS) on the thrombus for rest (a), exercise (b), and high exercise (c) flow conditions

inflow from the left and right iliac veins combines in the infrarenal portion of the IVC and develops rapidly in the lower portion of the vessel. In the present model, inflow rates from both iliac veins are assumed equal, though flow through the infrarenal IVC is asymmetric due to the vessel geometry. In contrast, flow through the unoccluded,

infrarenal IVC under exercise conditions (Fig. 2b–c) is more asymmetric and the asymmetry may induce larger shear forces on thrombus that is trapped by a filter, thereby facilitating thrombolysis (Fig. 2e–f). From Fig. 4, for example, the peak WSS on the model thrombus is approximately seven times larger for exercise conditions

Fig. 5 Contours of turbulent kinetic energy (*TKE*) for rest (a, d), exercise (b, e), and high exercise (c, f) flow conditions. Unoccluded vessels are in the top row (a–c), and partially occluded vessels are in the bottom row (d–f)



than rest conditions, and the larger wall shear stresses may help break-up trapped thrombus. To illustrate further the different flow profiles under rest and exercise conditions and their development in the infrarenal IVC, cross-sectional velocity contours are shown in Fig. 7. As evident, the velocity profile immediately downstream of the iliac bifurcation develops rapidly for both rest and exercise conditions. For rest conditions, a symmetric velocity profile that resembles a parabolic inlet is observed, and this profile propagates downstream until reaching the model thrombus. For exercise conditions, however, the velocity contours indicate an asymmetric flow pattern that propagates downstream until reaching the model thrombus. The asymmetry in the flow, which is due to asymmetric inflow from the iliac veins that is not damped by viscosity due to the relatively large Reynolds number (in comparison to rest conditions), may facilitate clot resolution and the development of unbalanced forces on the clot and IVC filter that may cause movement. It should be noted that in a real vessel, which contains more complex topology and

surrounding vessels, the iliac inflow into the IVC may be less symmetric than the current model due to anatomic variances and variable inflow rates, and flow asymmetries may be more pronounced under exercise conditions. Consequently, flow through the infrarenal IVC may not be fully developed near thrombus trapped by IVC filters.

Stagnant and recirculating flow are not the only factors that determine the risk of thrombosis in the IVC. In particular, stagnant flow is observed downstream of renal inflow, and the volume of stagnant flow increases with thrombus and exercise. As noted in Ref. [34], stagnant/recirculating flow are natural flow phenomena that occur superior to the bilateral renal vein inflows, and these flow conditions may be thrombogenic as a result of thrombin and fibrin accumulation [17]. Consequently, large portions of the suprarenal IVC that are exposed to stagnant/recirculating flow, especially under exercise conditions and partial occlusion (e.g., Fig. 2b, e), may elevate the risk of thrombosis. To understand the potential clinical significance of these flow conditions in the absence of in vivo

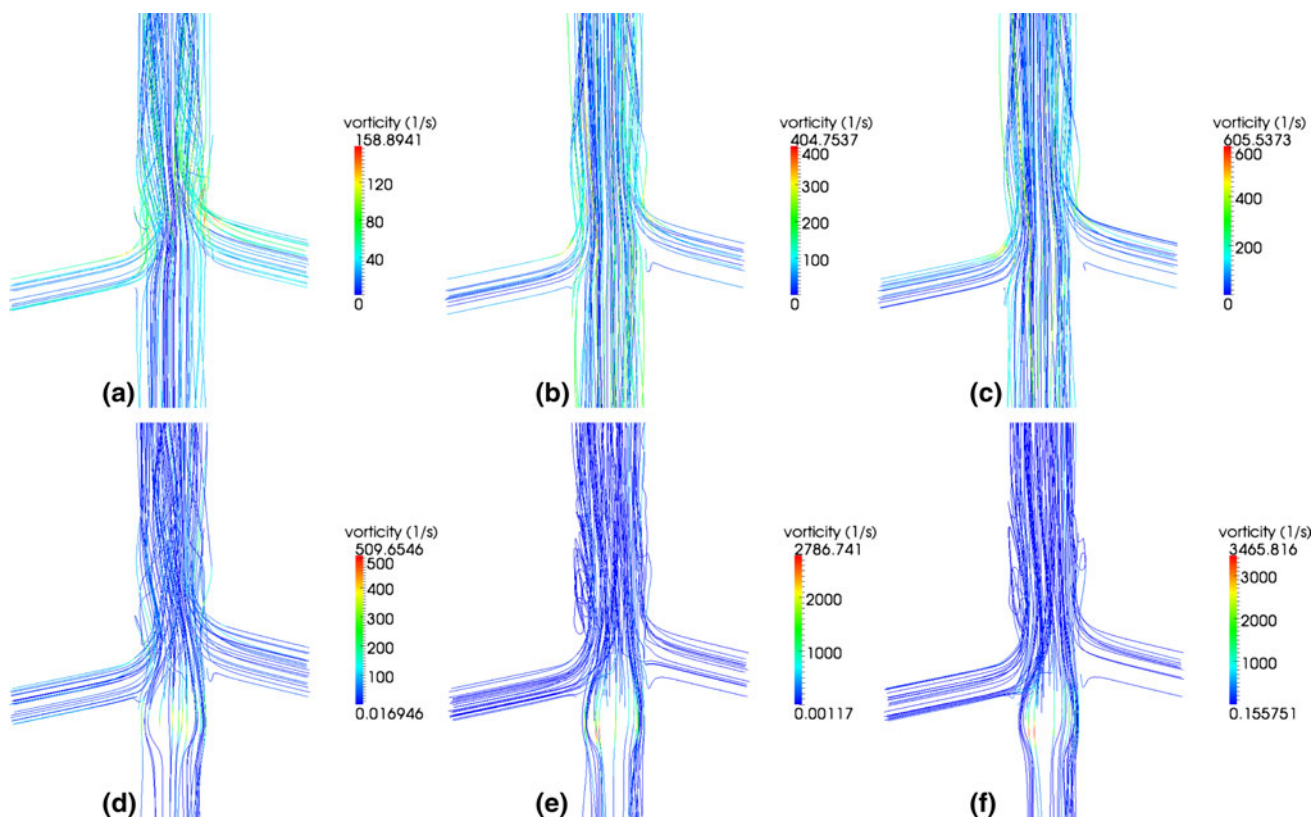
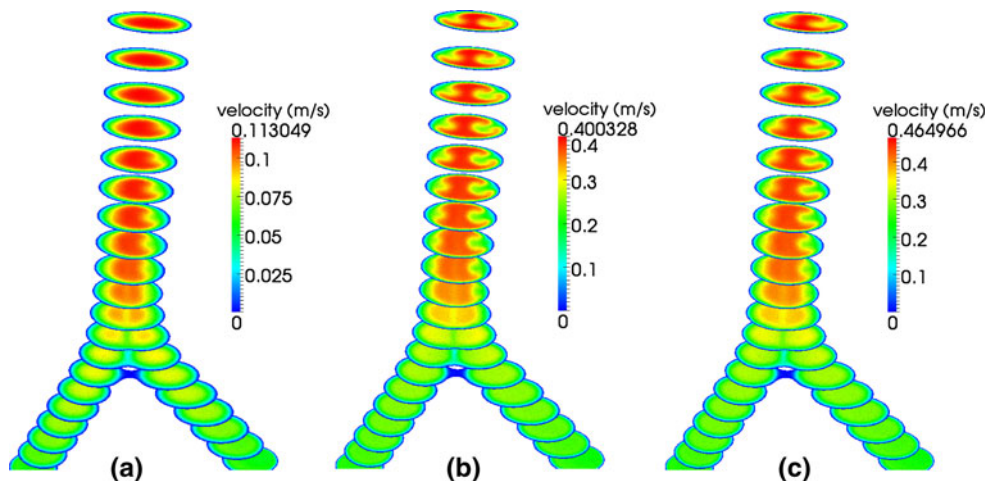


Fig. 6 Streamlines, colored by vorticity, for rest (a, d), exercise (b, e), and high exercise (c, f) flow conditions. Unoccluded vessels are in the *top row* (a–c), and partially occluded vessels are in the *bottom row* (d–f)

Fig. 7 Velocity contours on cross-sectional slices in the infrarenal IVC under three flow conditions: a rest, b exercise, and c high exercise



data, contrast the volumes of stagnant flow for the unoccluded vessel under rest and exercise conditions (i.e., Fig. 2a–c) with the corresponding volumes of stagnant flow for the partially occluded vessel (i.e., Fig. 2d–f). If the unoccluded flow patterns are considered natural and therefore at minimal risk of thrombus formation, then a qualitative comparison of flow through the non-occluded and partially occluded IVC suggests an elevated risk of suprarenal thrombosis for the partially occluded IVC under

sustained exercise conditions. Clinically, however, suprarenal thrombosis is exceptionally rare [9], which is consistent with the fact that exercise flow conditions may not be sustained over long enough time to induce clinically significant flow disruption in a partially occluded IVC. Further, the lack of clinical correlation between stagnant/recirculating flow and suprarenal thrombosis indicates that these flow conditions observed in the computational model are not the only factors that determine the risk of

thrombosis. Indeed, other physiological (e.g., vessel topology) and flow (e.g., flow unsteadiness and residence time, WSS) factors must also be considered when assessing the risk of thrombosis.

Large wall shear stresses observed for exercise conditions may be large enough to initiate thrombotic-like behavior, which may further occlude the vessel. As reported in Refs. [3, 30], thrombotic-like behavior may be induced by the imposition of shear forces on the order of 5–10 N/m². For the partially occluded vessel under exercise conditions, the WSS in the vicinity of the clot is 8–12 N/m², which is well within the range of initiation. There are, of course, additional factors to consider when assessing the risk of thrombosis, as discussed above. The duration of exposure time, for example, plays a role in determining platelet activation, which impacts the formation and growth of thrombus [36]. In the context of multi-hour exposure, for example, endothelium appears to be more actively antithrombotic under moderate shear conditions (e.g., 1.5 N/m²) and more fibrinolytic under high shear conditions (e.g., 3 N/m²) [7]. In addition, flow pulsatility can alter vessel response. In light of the remarks above, however, it should be noted that venous endothelial response is very different from arterial response, particularly for large veins such as the IVC [5]. Further, venous cellular signaling pathways are lost once they are fistulized, so data from vein grafts are not directly applicable [13]. Hence, additional investigation is needed to assess the clinical risk associated with moderate to intense physical activity when the IVC is partially occluded.

Thrombolysis may be accelerated during exercise due to larger wall shear stresses on the thrombus. As illustrated in Fig. 4, the peak WSS on the model thrombus is approximately 1.8, 12, and 15 N/m² for rest, exercise, and high exercise conditions, respectively. By comparison, exposure of platelets to shear stresses greater than 10 N/m² results in platelet lysis, and shear stresses as low as 5 N/m² result in platelet degranulation [6]. Consequently, the larger peak and average wall shear stresses observed during exercise may facilitate the break-up of thrombus trapped in vena cava filters. However, the current model treats the thrombus as rigid and impermeable. In contrast, thrombus are known to be deformable and porous in many situations, and these characteristics will likely facilitate morphing of clots into shapes that reduce the peak shear stresses. As a result, additional studies that focus on venous thrombus are required to assess the clinical significance of the shear stresses computed in this study.

There are no significant regions of transitional flow for the rest and exercise conditions considered in this study. As illustrated in Fig. 5, the turbulent kinetic energy contained in the flow field under rest conditions is several orders of magnitude smaller than the kinetic energy contained in the

total flow field (as indicated, for example, by the square of the velocity in Fig. 2). For the case of the partially occluded IVC during exercise and high exercise, there are regions of relatively large TKE immediately downstream of the model thrombus (Fig. 5e–f). These small regions of high TKE are consistent with relatively high turbulence intensity factors observed downstream of trapped thrombus in other computational models [22]. In all cases, the localized regions of relatively high TKE are small, isolated, and non-influential to the bulk flow. That is, due to the relatively low Reynolds number of the flow immediately downstream of the thrombus, turbulent fluctuations are quickly damped by viscosity, and the bulk flow remains laminar.

From a clinical perspective, understanding the hemodynamics of blood flow in the unoccluded and partially occluded IVC is important for optimization of IVC filter position. A previous computational modeling study evaluated the impact of filter placement and renal vein inflow on filter location [34]. This modeling study found that IVC filters placed in a near-juxtarenal position, so that thrombi are trapped near the renal vein inflow, likely confers increased levels of mechanical lysis on trapped thrombi. However, this previous study focused exclusively on modeling flow through the IVC under rest conditions, where the possibility of transitional or turbulent flow is smaller than under exercise conditions. Nonetheless, the results of that study sparked debate among clinicians as to whether turbulent flow characteristics have a significant impact on flow in the vicinity of renal inflow, even under rest conditions [23, 25]. Results of the current study clearly indicate that, even under rigorous exercise conditions, there is no evidence of significant regions of transitional or turbulent flow in the infrarenal, juxtarenal, or suprarenal IVC: the bulk flow is laminar. These findings further contribute to understanding and determining the optimal positions for both infrarenal and suprarenal placement of IVC filters.

The present modeling methodology may also provide a platform for understanding other venous thrombotic pathologies. That is, a thorough characterization of WSS and blood flow (laminar, transitional, and turbulent) in the IVC and its direct tributaries, may identify regions of abnormal flow that elevate the risk of a physiological response. May–Thurner syndrome, a condition defined by left common iliac vein stenosis/potential iliofemoral thrombosis due to the anatomic compression of the left iliac vein by the crossing right common iliac artery, could be studied with the modeling techniques described here.

Follow-up efforts may incorporate more physiological modeling and relax some of the assumptions used in the present framework. In particular, all vessel walls and model thrombi in this work are assumed to be rigid. It is observed clinically, however, that vessels and thrombi are

not rigid, and they may deform in response to local forces caused by pressure gradients and shear stresses induced by the flow dynamics. In response to the high-speed flow and pressure gradient that occurs in the narrow passage between the vessel wall and a trapped thrombus, for e.g., the IVC may expand to enable flow to bypass the thrombus, or the thrombus may deform due to the shear stresses. Consequently, the rigid model assumptions used in this work may over-estimate the WSS and may be an upper-bound on the true physiological value. A computer model that accounts for the fluid-structure interaction (FSI) between the flow and the vessel/thrombus would provide a more realistic model.

Although flow through the IVC is pulsatile, the model assumes that the flow is statistically stationary (i.e., all statistics are invariant under a shift in time [21]). Compared to flow through the aorta, flow through the IVC is less pulsatile due to a damping of the pressure pulse by the time blood reaches the venous system [4]. Nonetheless, a computational model that incorporates flow unsteadiness may yield additional insight into oscillatory shear indices and residence/exposure times, which further characterize the risk of thrombosis and the likelihood of thrombolysis. When combined with a model for the FSI, unsteady computations could also quantify the impact of pulsatility and dynamic morphology of the IVC and surrounding vessels, which may help assess the risk of vessel damage or biochemical (e.g., platelet) response. It must be noted, however, that incorporating unsteadiness into a flow simulation that also models turbulence would require a more complex and computationally expensive flow model, e.g., unsteady Reynolds averaged Navier–Stokes, large-eddy simulation.

Flow disruptions caused by IVC filters lead to regions of high-velocity flow and elevated WSS, and the extent and magnitude of the flow disruptions increase during exercise. In comparing the computed flow characteristics with those known to be thrombogenic, it appears that under exercise conditions the partially occluded vessel contains a flow environment that may facilitate the formation and growth of thrombus along the wall of the vena cava, but additional studies are needed to realized the clinical significance. In addition, clots that are trapped by IVC filters are exposed to high WSS, which may promote thrombolysis and the resolution of trapped clots. For both rest and exercise conditions of the unoccluded and partially occluded IVC, transitional flow does not influence the flow significantly.

Acknowledgments The authors thank Professor James E. Moore Jr. for providing the vessel geometry used in this study. LLNL is operated by Lawrence Livermore National Security, LLC, for the DOE National Nuclear Security Administration under Contract No. DE-AC52-07NA27344.

Conflict of interest The authors declare no conflicts of interest.

References

1. ANSYS Fluent. <http://www.fluent.com>
2. ANSYS Fluent theory manual
3. Barstad RM, Roald HE, Cui Y, Turitto VT, Sakariassen KS (1994) A perfusion chamber developed to investigate thrombus formation and shear profiles in flowing native human blood at the apex of well-defined stenoses. *Arterioscler Thromb* 14(12):1984–1991
4. Cheng CP, Herfkens RJ, Taylor CA (2003) Inferior vena cava hemodynamics quantified in-vivo at rest and during cyclic exercises using magnetic resonance imaging. *Am J Physiol Heart Circ Physiol* 284:1161–1167
5. Eriksson EE, Karlof E, Lundmark K, Rotzius P, Hedin U, Xie X (2005) Powerful inflammatory properties of large vein endothelium in vivo. *Arterioscler Thromb Vasc Biol* 25:723–728
6. Esclamado RM, Carroll WR (1999) The pathogenesis of vascular thrombosis and its impact in microvascular surgery. *Head Neck* 21(4):355–362
7. Grabowski EF (1995) Thrombolysis, flow, and vessel wall interactions. *J Vasc Interv Radiol* 6(6 Pt 2 Suppl):25S–29S
8. Harlal A, Ojha M, Johnston KW (2007) Vena cava filter performance based on hemodynamics and reported thrombosis and pulmonary embolism patterns. *J Vasc Interv Radiol* 18:103–115
9. Kalva SP, Chlapoutaki C, Wicky S, Greenfield AJ, Waltman AC, Athanasoulis CA (2008) Suprarenal inferior vena cava filters: a 20-year single-center experience. *J Vasc Interv Radiol* 19(7):1041–1047
10. Katsamouris AA, Waltman AC, Delichatsios MA, Athanasoulis CA (1988) Inferior vena cava filters: in vitro comparison of clot trapping and flow dynamics. *Radiology* 166:361–366
11. Khanafer KM, Bull JL, Berguer R (2009) Fluid-structure interaction of turbulent pulsatile flow within a flexible wall axisymmetric aortic aneurysm model. *Eur J Mech B Fluids* 28:88–102
12. Kroll MH, Hellums JD, Mcintire LV, Schafter AI, Moake JL (1996) Platelets and shear stress. *Blood* 88:1525–1541
13. Kudo FA, Muto A, Maloney SP, Pimiento JM, Bergaya S, Fitzgerald TN, Westvik TS, Frattini JC, Breuer CK, Cha CH, Nishibe T, Tellides G, Sessa WC, Dardik A (2007) Venous identity is lost but arterial identity is not gained during vein graft adaptation. *Arterioscler Thromb Vasc Biol* 27:1562–1571
14. Leask RL, Johnston KW, Ojha M (2001) In vitro hemodynamic evaluation of the Simon nitinol vena cava filter: possible explanation of IVC occlusion. *J Vasc Interv Radiol* 12:613–618
15. Leask RL, Johnston KW, Ojha M (2004) Hemodynamic effects of clot entrapment in the TrapEase inferior vena cava filter. *J Vasc Interv Radiol* 15:485–490
16. Lee P, Raizada A, Ciocca R (2009) Growing utilization of IVC filter placement from 2001–2005: analysis of NIS. Presented at the Society for Clinical Vascular Surgery 2009 Meeting, March 18–21, 2009, Fort Lauderdale, FL
17. Lowe GD (2004) Virchow's triad revisited: abnormal flow. *Pathophysiol Haemost Thromb* 33:455–457
18. Lu PC, Lai HC, Liu JS (2001) A reevaluation and discussion on the threshold limit for hemolysis in a turbulent shear flow. *J Biomech* 34:1361–1364
19. Mackman N (2008) Triggers, targets and treatments for thrombosis. *Nature (London)* 451:914–918
20. Murphy EH, Johnson ED, Arko FR (2008) Evaluation of wall motion and dynamic geometry of the inferior vena cava using intravascular ultrasound: implications for future device design. *J Endovasc Ther* 15:349–355
21. Pope SB (2000) *Turbulent Flows*. Cambridge University Press, UK
22. Rahbar E, Mori E, Moore JE Jr (2011) Three-dimensional analysis of flow disturbances due to clots in vena cava filters. *J Vasc Interv Radiol* 22:835–842

23. Requarth JA (2011) Re: toward an optimal position of inferior vena cava filters: computational modeling of the impact of renal vein inflow with the Celect and TrapEase filters. *J Vasc Interv Radiol* 22(1):102–103
24. Singer MA, Henshaw WD, Wang SL (2009) Computational modeling of blood flow in the TrapEase inferior vena cava filter. *J Vasc Interv Radiol* 20:799–805
25. Singer MA, Wang SL (2011) Modeling blood flow in a tilted inferior vena cava filter: does tilt adversely affect hemodynamics? *J Vasc Interv Radiol* 22:229–235
26. Stein PD, Sabbah HN (1974) Measured turbulence and its effect on thrombus formation. *Circ Res* 35:608–613
27. Stewart SF, Robinson RA, Nelson RA, Malinauskas RA (2008) Effects of thrombosed vena cava filters on blood flow: flow visualization and numerical modeling. *Ann Biomed Eng* 36:1764–1781
28. Stoneham GW, Burbridge BE, Millward SF (1995) Temporary inferior vena cava filters: in vitro comparison with permanent IVC filters. *J Vasc Interv Radiol* 6:731–736
29. Swaminathan TN, Hu HH, Patel AA (2006) Numerical analysis of the hemodynamics and embolus capture of a Greenfield vena cava filter. *J Biomech Eng* 128:360–370
30. Turitto VT, Hall CL (1998) Mechanical factors affecting hemostasis and thrombosis. *Thromb Res* 92(6 Suppl 2):S25–S31
31. Wakefield TW, Caprini J, Comerota AJ (2008) Thromboembolic disease. *Curr Probl Surg* 45:844–899
32. Walters DK, Cokljat D (2008) A three-equation eddy-viscosity model for Reynolds-averaged Navier–Stokes simulations of transitional flow. *J Fluids Eng* 130(12):121401
33. Wang SL, Timmermans HA, Kaufman JA (2007) Estimation of trapped thrombus volumes in retrievable inferior vena cava filters: a visual scale. *J Vasc Interv Radiol* 18:273–276
34. Wang SL, Singer MA (2010) Toward an optimal position for inferior vena cava filters: computational modeling of the impact of renal vein inflow with Celect and TrapEase filters. *J Vasc Interv Radiol* 21:367–274
35. Wang SL, Singer MA (2011) Drs. Wang and Singer respond. *J Vasc Interv Radiol* 22(1):103–105
36. Zhang JN, Bergeron AL, Yu Q, Sun C, McBride L, Bray PF, Dong JF (2003) Duration of exposure to high fluid shear stress is critical in shear-induced platelet activation-aggregation. *Thromb Haemost* 90(4):672–8